XI International Conference on Computational Plasticity. Fundamentals and Applications
COMPLAS XI
E. Oñate, D.R.J. Owen, D. Peric and B. Suárez (Eds)

RAPID MULTIAXIAL HIGH CYCLE FATIGUE LIMIT PREDICTIONS USING SELF-HEATING-BASED PROBABILISTIC MULTISCALE MODELS

MARTIN PONCELET[*], CEDRIC DOUDARD[†], SYLVAIN CALLOCH[†], BASTIEN WEBER[††] AND FRANCOIS HILD[*]

[*] LMT-Cachan (ENS Cachan/CNRS/Université Paris 6/PRES UniverSud Paris)
61 avenue du Président Wilson, F-94235 Cachan Cedex, France
Email: poncelet@lmt.ens-cachan.fr, hild@lmt.ens-cachan.fr, www.lmt.ens-cachan.fr

[†] LBMS EA 4325 (E.N.S.I.E.T.A./Université de Brest/E.N.I.B.)
2 rue François Verny, F-29806 Brest Cedex, France
Email: cedric.doudard@ensieta.fr, sylvain.calloch@ensieta.fr, www.ensieta.fr/lbms/

[††] ArcelorMittal Maizières Research
Voie Romaine BP 30320, F-57283 Maizières-lès-Metz, France
Email: bastien.weber@arcelormittal.com, www.arcelormittal.com

Key words: Thermomechanical process, Probability, Metallic materials, Multiaxial Fatigue.

Summary Thermal measurements under multiaxial cyclic loadings are used herein to predict multiaxial fatigue properties. Two models describing random microplasticity activation via a Poisson Point Process. The thermal response is interpreted as the "mean" behaviour of the microplastic activity, whereas the fatigue limit relies on the weakest link assumption. The first model is based upon a yield surface approach to account for stress multiaxiality at a microscopic scale. The second one relies on a probabilistic modelling of microplasticity at the scale of slip-planes. Both models are identified on thermal results and a uniaxial mean fatigue limit, and then validated using fatigue limits as well as thermal responses in the case of tension-torsion loadings on tubular specimens made of medium carbon steel. They predict well hydrostatic stress, volume and proportional multiaxial effects. The model with microplasticity described at the scale of slip-planes also offers a good prediction of non-proportional mean fatigue limits (~ 5% error) whereas the other model is less predictive (~ 17% error).

1 INTRODUCTION

The thermal measurements under cyclic loadings, usually referred to as "self-heating tests," [1-10] offer a neat and pragmatic way to predict high cycle fatigue properties without the drawback of the long-lasting traditional fatigue tests. Several models, from early empirical to recent approaches [11] based on microplasticity activation have been proposed to better understand and consolidate this link.

This paper focuses on two of these two-scale models developed for multiaxial loadings.

The first model is based upon a yield surface approach [12,13] to account for stress multiaxiality at a microscopic scale. The second one relies on a probabilistic modelling of microplasticity at the scale of slip-planes [14-16].

Both probabilistic descriptions are based on a Poisson Point Process. With this type of approach, the thermal response is linked to the "mean" behaviour of the microplastic activity, whereas the fatigue limit relies on the weakest link assumption. For the presented models, this implies that the fatigue limit is eventually described by a well-known Weibull model, which directly explains the influence of the stress heterogeneity and the volume effect on the fatigue results. From a thermal point of view, the influence of the stress heterogeneity is also taken into account, but with different formulae. Last, the influence of the hydrostatic stress is also described, thanks to the chosen intensity of the Poisson Point Process. For the first model, this intensity depends on the mean hydrostatic stress, and the normal stress to the considered plane for the second model.

Both models are validated using fatigue limits as well as thermal responses in the case of tension-torsion loadings on tubular specimens made of medium carbon steel. Both thermal effects and mean fatigue limit predictions are in good agreement with experimental results for proportional and non-proportional tension-torsion loadings. The conceptual difference between the two models implies a major difference of prediction capacity when non-proportional loadings are concerned, the mean fatigue limit prediction error of the critical shear stress approach being three times less than that with the yield surface approach. A notable advantage of the proposed models is that their identifications do not require non-proportional fatigue results, though they can predict them.

2 PROBABILISTIC BASIS OF THE MODELS

In metallic polycrystalline alloys, the physical process of damage initiation is usually governed by intragranular microplasticity. At that scale, the microplastic activity is not homogeneous because of local stress fluctuations (grain orientation and surrounding influence) and local plastic threshold. To model the onset of microplasticity, a set of elastoplastic sites randomly distributed within an elastic matrix is considered. For the sake of simplicity, no spatial correlation is considered herein. HCF damage is assumed to be localized at the mesoscopic scale and is induced by microplastic activity (in the grains whose orientation is favourable). The distribution of active sites (*i.e.*, sites where microplasticity occurs) of volume V_s is modelled by a Poisson Point Process [17-21]. The probability of finding k active sites in a domain Ω of volume V reads

$$P_k^*(\Omega) = \frac{\left[-\lambda^* V\right]^k}{k!} exp\left[-\lambda^* V\right] \tag{1}$$

where λ^* is the intensity of the Poisson Point Process and $\lambda^* V$ is the mean number of active sites. The intensity of the process depends on the loading level, and its form is detailed later.
The relationship between the stress tensor in a site where microplasticity occurs, $\underline{\underline{\sigma}}$, and the macroscopic stress tensor $\underline{\underline{\Sigma}}$ is given by the localisation law [22,23]

$$\underline{\underline{\sigma}} = \underline{\underline{\Sigma}} - 2\mu\left(1-\beta\right)\underline{\underline{\varepsilon_p}} \tag{2}$$

where $\underline{\underline{\varepsilon}}^p$ is the corresponding plastic strain tensor (assumption of additive decomposition of strain with an elastic and a plastic part) and μ the shear modulus. β is given by Eshelby's analysis of a spherical inclusion in an elastic matrix [24].

3 ELASTOPLASTIC BEHAVIOUR

3.1 Yield surface approach

The assumptions of the first model are chosen so that it presents a reduced number of parameters and closed-form formulae as its uniaxial predecessor [4]. Microplasticity is modelled at a microscopic scale and is described by a yield surface, normality rule and linear kinematic hardening

$$\begin{aligned} &\mathrm{f} = \mathrm{J}_2\left(\underline{\underline{\mathrm{S}}} - \underline{\underline{\mathrm{X}}}\right) - \sigma_{\mathrm{y}} \le 0 \\ &\dot{\underline{\underline{\varepsilon}}}^{\mathrm{p}} = \dot{\chi}\,\frac{\partial \mathrm{f}}{\partial \underline{\underline{\mathrm{S}}}} \\ &\dot{\underline{\underline{\mathrm{X}}}} = \frac{2}{3}\,\mathrm{C}\,\dot{\underline{\underline{\varepsilon}}}^{\mathrm{p}} \quad \textit{and} \quad \underline{\underline{X}}\left(\underline{\underline{\varepsilon}}^{p} = \underline{\underline{0}}\right) = \underline{\underline{0}} \end{aligned} \tag{3}$$

where J_2 is the second stress invariant, $\underline{\underline{\mathrm{S}}}$ the deviatoric stress tensor, $\underline{\underline{\mathrm{X}}}$ the back stress, C the hardening parameter, σ_y the yield stress and $\dot{\chi}$ the plastic multiplier.

The magnitude of the intrinsic dissipated energy $\delta\left(\Sigma_0^{eq}, \sigma_y\right)$ in a site over a loading cycle is calculated for a given value of the yield stress, von Mises' equivalent stress amplitude $\Sigma_0^{eq} = \max_t J_2\left(\underline{\underline{\Sigma}}(t) - \underline{\underline{\Sigma}}_m\right)$, and a mean stress $\underline{\underline{\Sigma}}_m$ given by

$$\underline{\underline{\Sigma}}_m = \underline{\underline{S}}_m + I_{1,m}\underline{\underline{I}} = \underset{Y}{Min}\left[\underset{t}{Max}\, J_2\left(\underline{\underline{\Sigma}}(t) - \underline{\underline{Y}}\right)\right] + \frac{1}{3}\underset{z}{Min}\left[\underset{t}{Max}\left(trace\left(\underline{\underline{\Sigma}}(t)\right) - z\right)\right]\underline{\underline{I}} \tag{4}$$

As for previous models proposed by the authors, the intensity of the Poisson Point Process describing the activation of microplasticity follows a power law of the equivalent stress amplitude

$$\lambda = \frac{1}{\mathrm{V}_0}\left(\frac{\Sigma_0^{eq}}{S_0 + \alpha I_{1,m}}\right)^m, \tag{5}$$

where α, m and $V_0 S_0^m$ are three material parameters, and $I_{1,m}$ the mean hydrostatic stress over a given cycle. Von Mises' equivalent stress amplitude is chosen because of the isotropy of the material tested hereafter. The power-law dependence is chosen because the onset of microplasticity follows a power-law of the applied stress [25] and because this form leads to a Weibull model when combined with the weakest link assumption [4,11]. The hydrostatic stress dependence is introduced to account for the mean stress effect on self-heating measurements and on fatigue properties.

It is now possible to calculate the global (mean) dissipated energy Δ in a domain Ω of

volume V, *i.e.*, first calculate the intrinsic dissipated energy $\delta\left(\Sigma_0^{eq},\sigma_y\right)$ of one site, integrate it over the whole population of active sites [11] to obtain the total dissipated energy $D\left(\Sigma_0^{eq}\right)$, and then integrate it over the whole domain Ω. In the case of uniform proportional loading, this calculation is straightforward and a closed-form solution is found [26]

$$\Delta = \frac{4\mathrm{m}\,\mathrm{V_S}}{\mathrm{h}(\mathrm{m}+1)(\mathrm{m}+2)}\frac{\left(\Sigma_{effdiss}\right)^{m+2}}{V_0\,S_0^m} \text{ with } \Sigma_{effdiss} = \frac{G_{m+2}^{1/(m+2)}\Sigma_{0M}^{eq}}{\left(1+\frac{\alpha}{S_0}I_{1,mM}\right)^{m/(m+2)}}, \tag{6}$$

where h is a parameter gathering the different thermal-related parameters.

This expression is identical to uniaxial homogeneous situation, except that uniaxial stress amplitude is changed to $\Sigma_{effdiss}$, the effective dissipative stress amplitude, where $\mathrm{G_{m+2}}$ is a *dissipation* heterogeneity factor. The latter factor can be calculated in the case of proportional loading

$$G_{m+2} = \frac{1}{\mathrm{V}}\int_\Omega \left(\frac{S_0+\alpha I_{1,mM}}{S_0+\alpha I_{1,m}(M)}\right)^m \left(\frac{\Sigma_0^{eq}(M)}{\Sigma_{0M}^{eq}}\right)^{\mathrm{m+2}} \mathrm{dV}, \tag{7}$$

and requires a numerical integration for non-proportional loadings.

3.2 Critical shear stress approach

From now on and for the sake of clarity, every variable of the present model having an equivalent in the yield surface approach is denoted with $\tilde{\cdot}$, *e.g.* Σ_0^{eq} and $\tilde{\Sigma}_0^{eq}$. Microplasticity is here modelled at the scale of slip planes based on Schmid's criterion

$$\tau - \tau_y \le 0, \tag{8}$$

with τ_y the critical shear stress and $\tau = \underline{\underline{\sigma}} : \underline{\underline{a}}$ the (resolved) shear stress for the considered direction defined by

$$\underline{\underline{a}} = \frac{1}{2}\left(\underline{n}^t\,\underline{m} + \underline{m}^t\,\underline{n}\right), \tag{9}$$

where $\underline{n}$ is the direction normal to the considered plane, and $\underline{m}$ the in-plane slip direction. The shear stress τ for the considered direction is related to the macroscopic shear stress T by the same localization law as before [15]

$$\tau = T - \mu(1-\beta)\gamma^p, \tag{10}$$

where γ^p is the plastic slip ($\underline{\underline{\varepsilon}}^p = \gamma^p\,\underline{\underline{a}}$). One direction thus becomes active when the shear stress amplitude T_0 is greater than the critical shear stress τ_y, which is assumed to be a random variable.

The same sequence of calculation is needed to express the global dissipated energy $\tilde{\Delta}$,

except that now an angular integration over all directions in space is necessary. The intensity of the Poisson Point Process follows a power law of the macroscopic shear amplitude integrated over all angular directions in space (defined by the solid angle Θ) [15]

$$\tilde{\lambda} = \frac{1}{\tilde{V}_0\left(\tilde{S}_0 + \tilde{\alpha}\, I_{1,max}\right)^{\tilde{m}}} \int \left(2T_0(\Theta)\right)^{\tilde{m}} d\Theta \quad , \tag{11}$$

where $\tilde{m}$, $\tilde{\alpha}$ and $\tilde{V}_0\left(\tilde{S}_0\right)^m$ are three parameters depending on the considered material, and $I_{1,max}$ the maximum hydrostatic stress over a given cycle. The global dissipated energy $\tilde{\Delta}$ is expressed in a similar way as for the first model

$$\tilde{\Delta} = \frac{4\tilde{m}\,\tilde{V}_S}{\tilde{h}(\tilde{m}+1)(\tilde{m}+2)} \frac{\left(\tilde{\Sigma}_{effdiss}\right)^{\tilde{m}+2}}{\tilde{V}_0\,\tilde{S}_0^{\tilde{m}}} \text{ with } \tilde{\Sigma}_{effdiss} = \frac{\tilde{G}_{\tilde{m}+2}^{1/(\tilde{m}+2)}\tilde{\Sigma}_{0M}^{eq}}{\left(1+\frac{\tilde{\alpha}}{\tilde{S}_0} I_{1,\max M}\right)^{\tilde{m}/(\tilde{m}+2)}}, \tag{12}$$

where $\tilde{h}$ is a parameter gathering the different thermal-related parameters of the model. The dissipation heterogeneity factor is defined as

$$\tilde{G}_{\tilde{m}+2} = \frac{1}{V}\int_{\Omega}\left(\frac{\tilde{S}_0 + \tilde{\alpha} I_{1,\max M}}{\tilde{S}_0 + \tilde{\alpha} I_{1,\max}(M)}\right)^{m}\left(\frac{\tilde{\Sigma}_0^{eq}(M)}{\tilde{\Sigma}_{0M}^{eq}}\right)^{\tilde{m}+2}\Gamma(\tilde{m}+2)\,dV \text{ with } \kappa(\tilde{m}+2) = \int\left(\frac{2T_0(M,\Theta)}{\tilde{\Sigma}_0^{eq}(M)}\right)^{\tilde{m}+2} \tag{13}$$

where $\kappa(\tilde{m}+2)$ represents the distribution of activated directions.

The definitions of equivalent stresses are not the same for the two models (Σ_0^{eq} is von Mises' equivalent stress, whereas $\tilde{\Sigma}_0^{eq}$ is Tresca's equivalent stress). Moreover the expression of $\tilde{G}_{m+2}$ is different from G_{m+2} since it includes the integration of the distribution of activated directions. This implies a numerical calculation, and a complete closed-form solution is no longer available. Aside from this little drawback, the hypotheses of this model make it intrinsically more relevant from a non-proportional point of view as will be shown in the next sections.

4 SELF-HEATING RESPONSE

The thermal response of the model corresponds to the "mean" point of view of the previous described microplastic onset, *i.e.*, the temperature is linked to the global dissipated energy. The * notation is used in the following equations of the section to clarify that they may be used for any of the two models (heat conduction equation is the same in both cases). Since the uniformity of the temperature in the specimen is a relevant assumption in the present case [27], the mean dissipation Δ^* is introduced in the following simplified heat conduction equation

$$\dot{\theta} + \frac{\theta}{\tau_{eq}} = \frac{f_r\,\Delta^*}{\rho\, c}, \tag{14}$$

where $\theta = T_{specimen} - T_{ref}$ is the mean temperature variation with respect to the reference temperature T_{ref}, τ_{eq} a characteristic time depending on the heat transfer boundary conditions [28], ρ the mass density, c the specific heat and f_r the loading frequency. The thermoelastic term is not considered since it vanishes over one cycle and only mean steady-state temperatures are needed. For both models, the mean (uniform) steady-state temperature $\bar{\theta}$ reads

$$\bar{\theta} = \eta^* \frac{m^*}{(m^*+1)(m^*+2)} \frac{\left(\Sigma_{effdiss}{}^*\right)^{m^*+2}}{V_0^* \left(S_0^*\right)^{m^*}} \text{ with } \eta^* = \frac{4 f_r \tau_{eq}}{\rho c} \frac{V_S^*}{h^*}. \tag{15}$$

This expression is similar to that for uniform tensile loading except for $\Sigma_{effdiss}{}^*$ term, and only three parameters are needed to describe the thermal response.

5 HIGH CYCLE FATIGUE RESPONSE

The weakest link theory is considered to describe the fatigue limit. The failure probability is then given by the probability of finding at least one active site in domain Ω. From Equation (1), the failure probability is thus given for both models by

$$P_F^* = 1 - exp\left[\int_\Omega -\lambda^* V \, dV\right]. \tag{16}$$

5.1 Yield surface approach

By using Equation (5), the failure probability is related to the loading amplitude

$$P_F = 1 - \exp\left[\int_\Omega -\frac{V}{V_0}\left(\frac{\Sigma_0^{eq}(M)}{S_0 + \alpha I_{1,m}(M)}\right)^m dV\right]. \tag{17}$$

which corresponds to Weibull's model [29,30]. This expression is simplified using a *stress* heterogeneity factor H_m, defined by

$$H_m = \frac{1}{V}\int_\Omega \left(\frac{\left(S_0 + \alpha I_{1,mM}\right)}{\left(S_0 + \alpha I_{1,m}(M)\right)} \frac{\Sigma_0^{eq}(M)}{\Sigma_{0M}^{eq}}\right)^m dV. \tag{18}$$

Equation (16) becomes

$$P_F = 1 - \exp\left[-\frac{V_{eff}}{V_0}\left(\frac{\Sigma_{0M}^{eq}}{S_0 + \alpha I_{1,mM}}\right)^m\right]. \tag{19}$$

where $V_{eff} = V H_m$ denotes the effective volume. From this expression, and as for the previous self-heating models proposed by the authors [4], the fatigue limit features are derived

$$\overline{(\Sigma_0^{eq})_\infty} = \overline{\Sigma}_\infty = \left(S_0 + \alpha I_{1,mM}\right)\left(\frac{V_0}{V_{eff}}\right)^{(1/m)} \Gamma\left(1+\frac{1}{m}\right) \text{ and } CV = \frac{\overline{\overline{\Sigma}}_\infty}{\overline{\Sigma}_\infty} = \frac{\sqrt{\Gamma\left[1+\frac{2}{m}\right] - \Gamma^2\left[1+\frac{1}{m}\right]}}{\Gamma\left(1+\frac{1}{m}\right)} \tag{20}$$

where $\overline{\Sigma}_\infty$ is the mean fatigue limit, $\overline{\overline{\Sigma}}_\infty$ the standard deviation and CV the coefficient of variation.

The stress H_m and dissipation G_{m+2} heterogeneity factors have intrisincally different meanings. However their expressions are very similar in the case of proportional loadings [see equations (18) and (7)]. Moreover the high value of the exponent m (m = 12 for the present material) induces very close values of these factors, even more for loadings with uniform mean hydrostatic stresses. This means that the combined effects of direction and heterogeneity of loading are nearly the same for fatigue and self-heating results, which makes easier the interpretation of self-heating results.

On the contrary, H_m and G_{m+2} can be very different for non-proportional loadings. Considering two uniform loadings with the same equivalent stress amplitude and the same mean hydrostatic stress, the first one proportional and the second one non-proportional, H_m factors are identical but G_{m+2} factors can be very different.

5.2 Critical shear stress approach

With the second model the failure probability corresponds to the probability of finding at least one active *slip direction* in the given volume. The failure probability is thus related to the shear stress amplitude by

$$\tilde{P}_F = 1 - \exp\left[-\frac{1}{\tilde{V}_0}\int_\Omega\int\left(\frac{2T_a}{\tilde{S}_0 + \tilde{\alpha} I_{1,max}}\right)^{\tilde{m}} d\Theta\, dV\right] . \tag{21}$$

A stress heterogeneity factor $\widetilde{H}_{\tilde{m}}$ is again introduced,

$$\widetilde{H}_{\tilde{m}} = \frac{1}{V}\int_\Omega\left(\frac{\left(\widetilde{S}_0 + \tilde{\alpha} I_{1,maxM}\right)}{\left(\widetilde{S}_0 + \tilde{\alpha} I_{1,max}(M)\right)}\frac{\widetilde{\Sigma}_0^{eq}(M)}{\widetilde{\Sigma}_{0M}^{eq}}\right)^{\tilde{m}} \kappa(\tilde{m})\, dV , \tag{22}$$

so that equation (20) becomes

$$\tilde{P}_F = 1 - \exp\left[-\frac{\tilde{V}_{eff}}{\tilde{V}_0}\left(\frac{\tilde{\Sigma}_{0M}^{eq}}{\tilde{S}_0 + \tilde{\alpha} I_{1,max}}\right)^{\tilde{m}}\right]. \tag{23}$$

Last the mean fatigue limit is expressed (CV is the same as for the previous model)

$$\overline{(\widetilde{\Sigma}_0^{eq})}_\infty = \overline{\widetilde{\Sigma}}_\infty = \left(\widetilde{S}_0 + \tilde{\alpha} I_{1,maxM}\right)\left(\frac{\widetilde{V}_0}{\widetilde{V}_{eff}}\right)^{(1/\tilde{m})} \Gamma\left(1+\frac{1}{\tilde{m}}\right). \tag{24}$$

Note that $\widetilde{G}_{\tilde{m}+2}$ and $\widetilde{H}_{\tilde{m}}$ are *a priori* different because of the influence of the hydrostatic stress. The values of these factors are however again nearly identical because of the high value of $\tilde{m}$ for proportional and non-proportional loadings.

The identication of m^* is performed using equation (15), so that the values of m and $\tilde{m}$ are identical, and so the relative fatigue scatter is the same for both models (*i.e.*, same *CV* value). The mean fatigue limits are different because equations (20) and (24) account for the influence of several parameters on fatigue properties in different ways.

6 EXPERIEMENTAL APPLICATION

Both models depend on three parameters to predict the fatigue limits, and a last one to account for self-heating under cyclic loadings. They are applied to the case of AISI 1045 medium carbon steel tubes under tension-torsion loadings. In that case, the macroscopic stress tensor depends only on the radius r of the specimen and is defined by

$$\Sigma_{zz} = \Sigma_{11,0}\sin(2\pi f_r t) + \Sigma_m \qquad (25)$$

$$\Sigma_{\theta z} = \Sigma_{12,0}\frac{r}{R_e}\sin(2\pi f_r t + \varphi)$$

where $\Sigma_{11,0}$ and $\sqrt{3}\,\Sigma_{12,0} = \tan(\phi)\,\Sigma_{11,0}$ are the tensile and shear stress amplitudes, φ the phase lag between shear and normal stresses, Σ_m the mean tensile stress, and R_e the external radius of the specimen. The hydrostatic pressure is uniform over the volume of the specimen, so that the two heterogeneity factors of the both models have the same expression for proportional loadings, *i.e.* $G_m = H_m$ and $\widetilde{G}_{\tilde{m}} = \widetilde{H}_{\tilde{m}}$. In the next section, the identification procedure is presented, and a comparison of predictions with experimental fatigue results.

6.1 Identification

Identification is based on self-heating curves obtained with the same procedure as for previous self-heating tests [4,11,12,27]. During the test, the amplitude of loading is step-wise constant, and increases once the differential temperature is stabilised. One pure torsion loading and one pure tension with non-zero mean stress are applied. The steady-state temperature is plotted as a function of the loading amplitude in Figure 1. As for other steels [4,11,12,27], each curve has a first part that shows virtually no change in temperature, whereas in the second part the temperature increases significantly with the stress amplitude. This transition is reported to be a rather good estimation of the mean fatigue limit for steels in uniaxial homogeneous case [4,6,7,8]. Moreover it has been shown that the gradual increase of temperature is linked to the fatigue scatter [4]. The relatively short duration of self-heating tests (in comparison with traditional fatigue tests) makes them not only interesting for academic studies, but also very attractive for industrial purposes.

Both models depend exactly on the same parameters, namely, m^* describes the scatter of fatigue results and the slope (in a log-log plot) of the self-heating temperature response, η^* a scale parameter for the thermal response, α^* accounts for the effect of the mean hydrostatic stress on self-heating and fatigue properties, and $V_0^*\left(S_0^*\right)^{m^*}$ the scale parameters for the fatigue

response. All parameters are identified using the 2 self-heating tests and one fatigue limit that may concern any type of geometry or loading. Figure 1 shows the identification for both approaches.

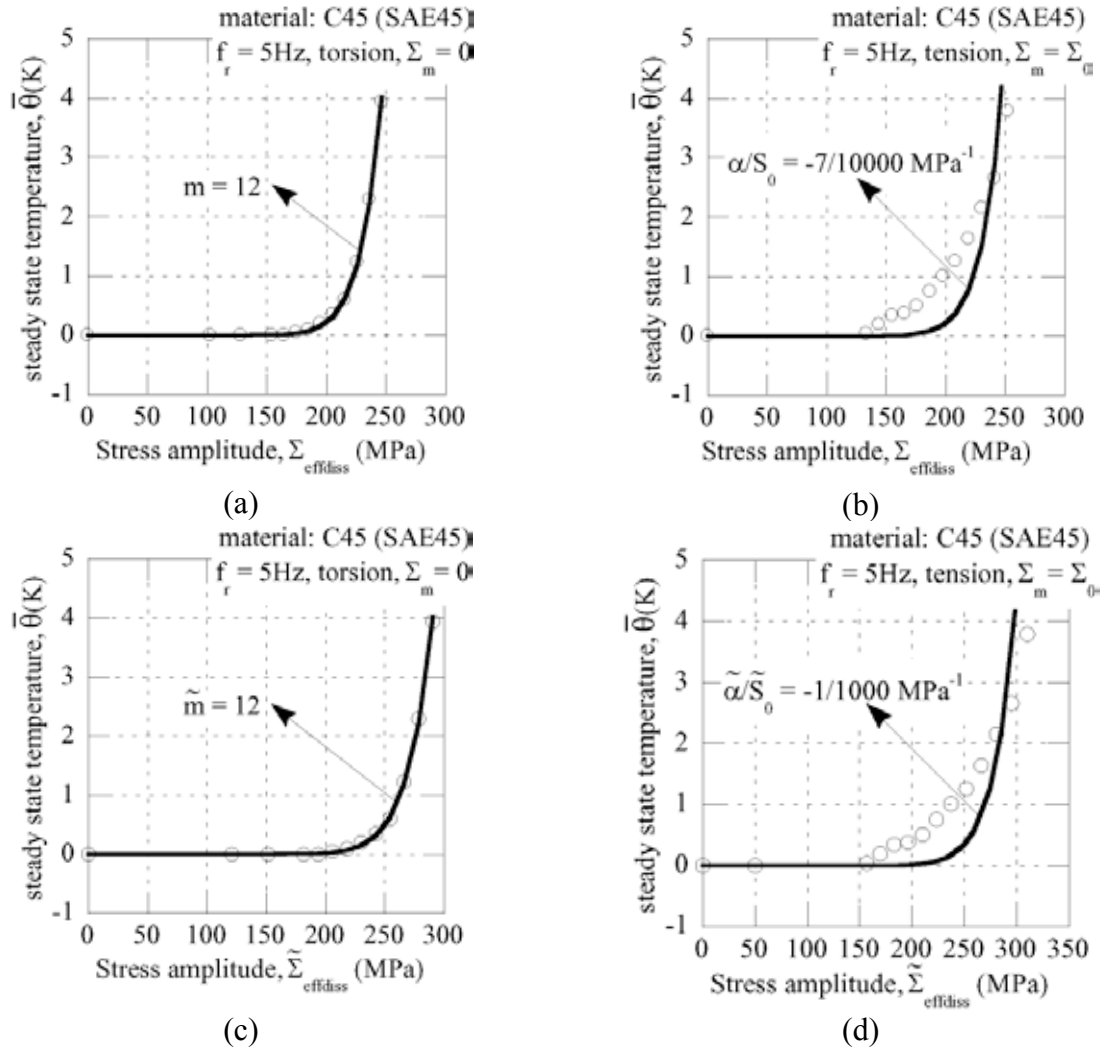

Figure 1: Identification of m and α using torsion (a) and tension with mean stress (b) self-heating curves. Identification of $\tilde{m}$ (c) and $\tilde{\alpha}$ (d) using the same curves.

No non-proportional loading results are needed for this identification. Any couple of loading paths may be used to identify parameters m^*, η^* and α^* as long as their mean (resp. maximum) hydrostatic stresses over a given cycle are different.

The last (scale) parameter of each model is obtained by using a mean fatigue limit and Equation (20) for the yield surface approach, or Equation (24) for the critical shear stress approach. This value is obtained for tensile loadings ($\phi = 0°$ and $\Sigma_m = 0$) when fatigue limits are evaluated for 5×10^6 cycles. Staircase tests are performed on 15 smooth and round

samples machined from the same steel bar as before. Stress steps are equal to 10 MPa. The measured mean fatigue limit is 262 MPa.

6.2 Validation

Models are first validated from a thermal point of view. A pure tension (zero mean stress) and a non-proportional (constant von Mises' equivalent stress at mean radius ($\phi = 48°$, $\varphi = 90°$)) self-heating tests are performed. Figure 2 shows self-heating curves as a function of von Mises (a), yield surface (b) and critical shear stress (c) equivalent stress amplitudes. For both models all curves collapse onto one another when the definition of the equivalent stress is used. This result means that both hydrostatic stress and non-proportional thermal effects are well predicted.

Mean fatigue limit prediction is then checked using three different series of staircase tests (target: 5 x 10^6 cycles). The first one is a pure torsion loading, the second one a proportional loading ($\phi = 48°$ and $\Sigma_m = 0$) and last one a non-proportional loading ($\phi = 48°$, $\varphi = 90°$). Comparison between experimentally obtained mean fatigue limits and predicted ones is shown in Table 1, using the relative prediction error defined as $\left(\overline{\Sigma}_\infty^{exp} - \overline{\Sigma}_\infty^{pre}\right)\Big/\overline{\Sigma}_\infty^{exp}$. Predictions are in good agreement with experimental results, except for the yield surface model, which is non-conservative for non-proportional loading.

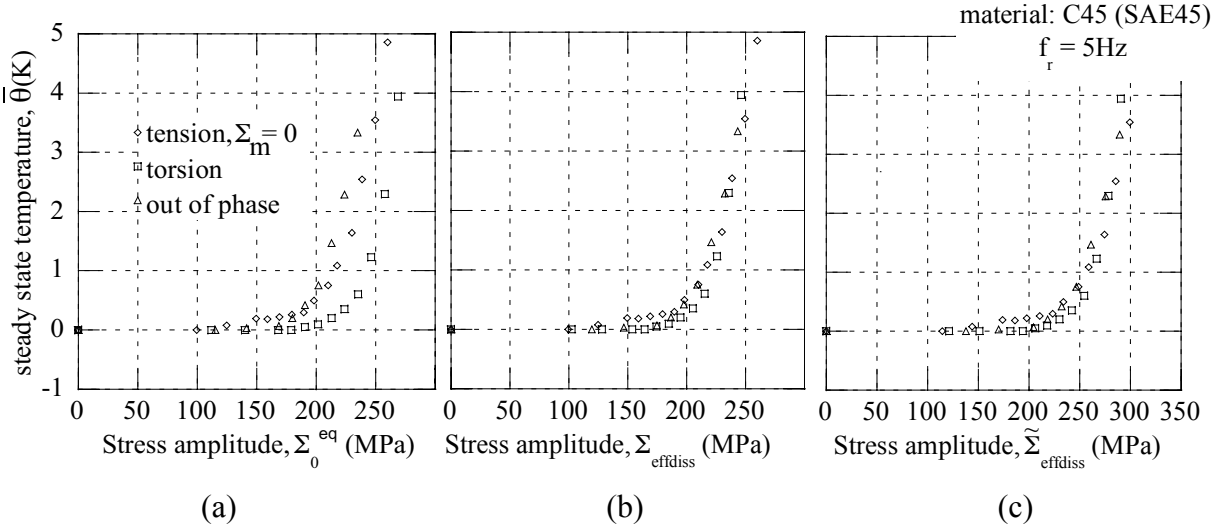

Figure 2: Thermal validation: self-heating curves for different equivalent stress amplitude.

Table 1: Fatigue validation. Relative prediction errors of both models.

Loadings ($\Sigma_m = 0$)	Prop. ($\phi = 90°$)	Prop. ($\phi = 48°$)	N-prop. ($\phi = 48°$, $\varphi = 90°$)
Σ_0^{eq} (MPa)	277	267	205
Critical shear stress model	6%	7%	-5%
Yield surface model	9%	6%	-17%

7 CONCLUSION

The present paper was focused on a comparison of two multiscale models whose parameters are tuned thanks to self-heating data, and subsequently used to predict multiaxial high cycle fatigue properties. The first model uses an equivalent stress to account for stress multiaxiality at the microscopic scale, whereas the second one relies on a description of microplasticity at the scale of slip-planes.

Both thermal and fatigue behaviours are well described by each model. They account for the influence of the stress heterogeneity, the volume effect and the hydrostatic stress. Relative errors are small for each experimental validation, even though the "identification cost" is low (and the same for each model), thanks to the information extracted from the self-heating tests.

The distinction between the yield surface and critical shear stress approaches is nearly impossible from a thermal point of view (see Figures 2 (b) and (c)), whereas an important difference appears as along as non-proportional fatigue limit is concerned. The interest of the critical shear stress approach is clearly shown, lowering (in absolute value) the prediction error from –17% to –5% without the addition of new parameters. This is due to its microplastic activation description, combining probabilistic onset and slip-planes approach, which leads to very close *dissipation* and *stress* heterogeneity factors.

A next step of this work will be the prediction of multiaxial fatigue life with the critical shear stress approach and the application to industrial cases.

REFERENCES

[1] Bérard, J.-Y., Rathery, S., and Béranger, A.-S., Détermination de la limite d'endurance des matériaux par thermographie infrarouge. *Mat. Techn*. (1998) **1-2**:55-57.

[2] Cura, F., Curti, G. and Sesana, R., A new iteration method for the thermographic determination of fatigue limit in steels. *Int. J. Fat.* (2005) **27[4]**:453-459.

[3] Dengel, D. and Harig, H., Estimation of the fatigue limit by progressively-increasing load tests. *Fat. Fract. Eng. Mat. Struct.* (1980) **3[1]:**113.

[4] Doudard, C., *Détermination rapide des propriétés en fatigue à grand nombre de cycles à partir d'essais d'échauffement*. PhD thesis, ENS Cachan, France, (2004).

[5] Galtier, A., Bouaziz, O. and Lambert, A., Influence de la microstructure des aciers sur leurs propriétés mécaniques. *Méc. Ind.* (2002) **3[5]**: 457-462.

[6] Krapez, J.-C., Pacou, D. and Bertin, C., Application of lock-in thermography to a rapid evaluation of the fatigue limit in metals. 5th AITA, Int. Workshop on Advanced Infrared Techn. and Appl., Venezia (Italy), ed. E. Grinzato et al. (1999), 379-385.

[7] La Rosa G. and Risitano, A., Thermographic methodology for rapid determination of the fatigue limit of materials and mechanical components. *Int. J. Fat.* (2000) **22[1]**: 65-73.

[8] Luong, M.P., Infrared thermographic scanning of fatigue in metals. *Nuclear Engineering and Design.* (1995) **158[2-3]**:363-376.

[9] Mabru, C. and Chrysochoos, A., Dissipation et couplages accompagnant la fatigue de matériaux métalliques. Photomécanique 2001, ed. Y. Berthaud, M. Cottron, J.-C. Dupré, F. Morestin, J.-J. Orteu and V. Valle, GAMAC, (2001) 375-382.

[10] Stromeyer, C.E., A machine for determining fatigue limits calorimetrically. *Rep. Brit. Ass.* (1915) 638.

[11] Doudard, C., Calloch, S., Cugy, P., Galtier, A. and Hild, F., A probabilistic two-scale model for high cycle fatigue life predictions. *Fat. Fract. Eng. Mat. Struct.* (2005) **28**:279-288.
[12] Doudard, C., Poncelet, M., Calloch, S., Boué, C., Hild, F. and Galtier, A., Determination of an HCF criterion by thermal measurements under biaxial cyclic loading, Int. J. Fatigue. (2007) **29[4]**:748-757.
[13] Lemaitre, J. and Doghri, I. Damage 90: a post processor for crack initiation. *Comput. Methods Appl. Mech. Engrg.* (1994) **115**: 197-232.
[14] Dang Van, K., *Sur la résistance à la fatigue des métaux. Sciences et techniques de l'armement*, Mémorial de l'artillerie française, 3ème fascicule (1973).
[15] Doudard, C., Hild, F., and Calloch, S., A probabilistic model for multiaxial high cycle fatigue. *Fat. Fract. Eng. Mat. Struct.* (2007) **30**:107-114.
[16] Morel, F., A fatigue life prediction method based on a mesoscopic approach in constant amplitude multiaxial loading. *Fat. Fract. Eng. Mat. Struct.* (1998) **21**:241-256.
[17] Curtin W.A., Exact Theory of Fiber Fragmentation in Single-Filament Composite, *J. Mater. Sci.* (1991), **26**:5239-5253.
[18] Gulino, R. and Phoenix, S.L., Weibull strength statistics for graphite fibres measured from the break progression in a model graphite/glass/epoxy microcomposite. *J. Mater. Sci.* (1991) **26**:3107-3118.
[19] Jeulin, D., *Modèles morphologiques de structures aléatoires et changement d'échelle*. thèse d'Etat, Université de Caen, France, (1991).
[20] Fedelich B., A stochastic theory for the problem of multiple surface crack coalescence, *Int. J. Fract.* (1998) **91**:23-45.
[21] Denoual, C. and Hild, F., Dynamic fragmentation of brittle solids: A multi-scale model. *Eur. J. Mech. A/Solids.* (2002) **21**:105-120
[22] Berveiller, M. and Zaoui, A., An extension of the self-consistent scheme to plastically flowing polycristals. *J. Mech. Phys. Solids.* (1979) **26**:325-344.
[23] Kröner, E., On the plastic deformation of polycristals. *Acta Met.* (1984) **9**:155-161.
[24] Eshelby, J.D., The Determination of the Elastic Field of an Ellipsoidal Inclusion and Related Problems. *Proc. Roy. Soc. London A.* (1957) **241**:376-396.
[25] Cugy, P. and Galtier, A., Microplasticity and temperature increase in low carbon steel, in: Proceedings of the 7th Int. Fat. Conf., Stockholm (Sweden), (2002).
[26] Poncelet, M., Doudard, C., Calloch, S., Weber, B. and Hild, F., Probabilistic multiscale models and measurements of self-heating under multiaxial high cycle fatigue, *Jal Mech. Phys. Sol.* (2010) **58**:578-593
[27] Poncelet, M., Doudard, C., Calloch, S., Hild, F., Weber, B. and Galtier, A., Prediction of self-heating measurements under proportional and non-proportional multiaxial cyclic loadings, *C. R. Mécanique.* (2007) **335**:81-86
[28] Chrysochoos, A. and Louche, H., An infrared image processing to analyse the calorific effects accompanying strain localisation, *Int. J. Engrg. Sci.* (2000) **38**:1759-1788,
[29] Weibull, W., A Statistical Theory of the Strength of Materials, *Roy. Swed. Inst. Eng. Res. (*1939) Report 151.
[30] Weibull, W., A statistical distribution function of wide applicability, *ASME J. Appl. Mech.* (1951) **18**:293-297.